Minimizing the Effects of Variable Cone Tip Diameters by Implementing the q_c*HMM* Algorithm on Cone Bearing Measurements

Erick Baziw, Ph.D.,P.Eng.[1] and Gerald Verbeek, B.Sc., M.Sc.[2]

[1] Baziw Consulting Engineers Ltd., 3943 West 32nd Avenue, Vancouver B.C., Canada V6S 1Z4; E-mail: ebaziw@bcengineers.com
[2] Baziw Consulting Engineers Ltd., 1411 Cumberland Road, Tyler, TX USA 75703; E-mail: gverbeek@bcengineers.com

ABSTRACT: The cone penetration test (CPT) is an extensively implemented geotechnical tool for assessing soil properties and mapping soil profiles. CPT consists of pushing at a constant rate an electronic penetrometer into penetrable soils and recording the resistance to the cone tip or cone bearing (q_c). The q_c values (after correction for the pore water pressure to get q_t) are utilized to characterize the soil profile along with measured sleeve friction. Cone bearing measurements at a specific depth are blurred or averaged due to q_c values being strongly influenced by soils within 10 to 30 cone diameters from the cone tip. This blurring of the true cone tip readings results in the inability to identify thin and low bearing soils which are masked by the properties of the adjacent soils. The cone tip diameter is directly related to the extent of blurring of the q_c values. A larger cone tip diameter will resulted in greater q_c blurring. The most common cone tips have associate areas of 5 cm^2, 10 cm^2 and 15 cm^2. The q_c*HMM* algorithm was developed to address the q_c blurring\averaging limitation. The q_c*HMM* algorithm implements a hidden Markov model smoother so that true cone bearing are obtained from the averaged/blurred q_c values. This paper illustrates how the q_c*HMM* algorithm can be implemented so that q_c profiles obtained from cones with varying cone tip diameters can be corrected to give consistent results.

INTRODUCTION

The Cone Penetration Test (CPT) is a geotechnical in-situ tool which is utilized to identify and characterize sub-surface soils (Lunne et al., 1997; Robertson, 1990; ASTM D6067, 2017). In addition, the CPT is utilize to estimate toe bearing capacity of piles (Eslami and Fellenius, 1995 and 1997). In CPT a steel cone is pushed vertically into the ground at a typical standard rate of 2cm per second and data are recorded at constant rate during penetration (typically every 1cm to

2cm). The cone penetrometer has electronic sensors to measure penetration resistance at the tip (q_m) and friction in the shaft (friction sleeve) during penetration. A CPTU probe is equipped with a pore-water pressure sensor and is called a piezo-cones. For piezo-cones with the filter element right behind the cone tip (the so-called u_2 position) it is standard practice to correct the recorded tip resistance for the impact of the pore pressure on the back of the cone tip. Figure 1 illustrates a schematic and the associated terminology of a cone penetrometer.

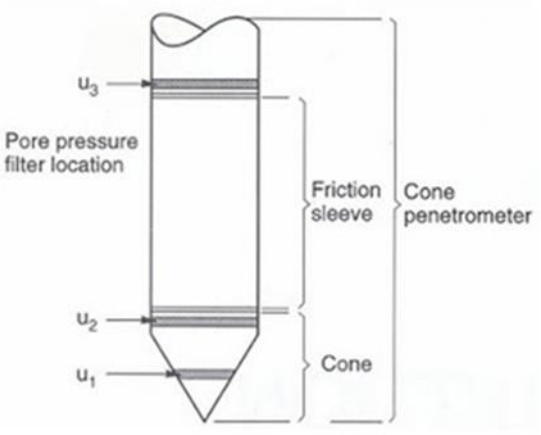

Fig. 1. Schematic and terminology for cone penetrometer (Lunne et al., 1997).

The cone tip resistance measured at a particular depth is affected by the values above and below the depth of interest which results in an averaging or blurring of the q_v values (Boulanger and DeJong, 2018; Robertson, 1990; Baziw and Verbeek, 2021, 2022a and 2022b). This phenomenon is especially of concern when mapping thin soil layers which is critical for liquefaction assessment. Mathematically the measured cone tip resistance q_c is described as (Baziw and Verbeek, 2021 and 2022)

$$q_c(d) = \sum_{j=1}^{60\times\left(\frac{d_c}{\Delta}\right)} w_c(j) \times q_v\left(\Delta_{qm} + j\right) + v(d) \qquad (1)$$

$$\Delta_{qc} = (d - \Delta_{wm}),\ \ \Delta_{wm} = 30 \times \left(\frac{d_c}{\Delta}\right)$$

where

d	cone depth (m)
d_c	cone tip diameter (m)
Δ	q_c sampling rate (m)
$q_c(d)$	measured cone penetration tip resistance (MPa)
$q_v(d)$	true cone penetration tip resistance (MPa)
$w_c(d)$	the $q_v(d)$ averaging function (dimensionless)
$v(d)$	additive noise, generally taken to be white with a Gaussian probability distribution function (PDF) (MPa)

In eq. (1) it assumed that w_c averages q_v over 60 cone diameters centered at the cone tip. Boulanger and DeJong (Boulanger and DeJong, 2018) outline how to calculate w_c below (after correcting the equation for w_1 (Baziw and Verbeek, 2021)):

$$w_c = \frac{w_1 w_2}{\sum w_1 w_2} \qquad (2a)$$

$$w_1 = \frac{C_1}{1 + \left|\left(\frac{z'}{z'_{50}}\right)^{m_z}\right|} \tag{2b}$$

$$w_2 = \sqrt{\frac{2}{1 + \left(\frac{q_{v,z'}}{q_{v,z'=0}}\right)^{m_q}}} \tag{2c}$$

where:

w_1 accounts for the relative influence of any soil decreasing with increasing distance from the cone tip.

w_2 adjusts the relative influence that soils away from the cone tip will have on the penetration resistance based on whether those soils are stronger or weaker.

z' the depth relative to the cone tip normalized by the cone diameter.

z'_{50} the normalized depth relative to the cone tip where $w_1 = 0.5\ C_1$.

C_1 equal to unity for points below the cone tip, and linearly reduces to a value of 0.5 for points located more than 4 cone diameters above the cone tip.

m_z exponent that adjusts the variation of w_1 with z'.

m_q exponent that adjusts the variation of w_2 with $\left(\frac{q_{v,z'}}{q_{v,z'=0}}\right)$.

Boulanger and DeJong (2018) provide a thorough outline and review on the setting of the parameters given in eq. (2) based upon extensive research and modelling. In general terms, soils in front of the cone tip have a greater influence on penetration resistance than the soils behind the cone tip. In the subsequently outlined test bed simulations the parameters in eq. (2) are set identical to those outlined by Boulanger and DeJong. In this case, exponents $m_q = 2$ and $m_z = 3$.

Baziw and Verbeek (2021, 2022a and 2022b) developed an algorithm to optimally obtain true q_v cone bearing estimates from blurred measurements q_c. The initial algorithm developed by Baziw and Verbeek (2021 and 2022a) (the so called q_c*HMM-IFM*) combined a Bayesian recursive estimation (BRE) Hidden Markov Model (HMM) filter with Iterative Forward Modelling (IFM) parameter estimation in a smoother formulation. In recent modifications and enhancements of the q_c*HMM* (Baziw and Verbeek, 2022b) it was possible to drop the IFM portion of the algorithm. This was predominantly accomplished by refining the HMM filter parameters. This paper briefly outlines the current q_c*HMM* algorithm formulation and presents the results from very challenging test bed simulations. The simulated cone bearing profiles are generated for a true cone bearing profile q_v where acquired measured values q_c are obtained by implementing eq. (1) for cone tip areas of 5cm^2, 10cm^2, and 15cm^2. The test bed simulations demonstrated that the q_c*HMM* algorithm gave nearly identical q_v values for the data acquired utilizing cone tip areas of 5cm^2, 10cm^2, and 15cm^2.

q_c*HMM* ALGORITHM FILTER FORMULATION

The HMM filter (also termed a grid-based filter) has a discrete state-space representation and has a finite number of states (Arulampalam et al., 2002). In the HMM filter the posterior PDF is represented by the delta function approximation as follows:

$$p(x_{k-1}|z_{1:k-1}) = \sum_{i=1}^{N_s} w_{k-1\backslash k-1}^{i}\delta\left(x_{k-1} - x_{k-1}^{i}\right) \quad (3)$$

where x_{k-1}^{i} and $w_{k-1|k-1}^{i}$, $i = 1,\ldots,N_s$, represent the fixed discrete states and associated conditional probabilities, respectively, at time index *k-1*, and N_s the number of particles utilized. In the case of the q_c*HMM* algorithm the HMM discrete states represent possible q_v values where maximum, minimum and resolution values are specified. The HMM governing equations are outlined in Table 1.

Table 1. HMM Governing Equations

STEP	DESCRIPTION	MATHEMATICAL REPRESENTATION	EQ.
1	Initialization (k=0) – initialize particle weights.	e.g., $w_k^i \sim 1/N_s$, $i = 1,\ldots,N_s$.	(4)
2	Prediction - predict the weights.	$w_{k\backslash k-1}^{i} = \sum_{j=1}^{N_s} w_{k-1\backslash k-1}^{j} p\left(x_k^i | x_{k-1}^j\right)$	(5)
3	Update - update the weights.	$w_{k\backslash k}^{i} = \frac{w_{k\backslash k-1}^{i} p\left(z_k | x_k^i\right)}{\sum_{j=1}^{N_s} w_{k\backslash k-1}^{j} p\left(z_k | x_k^j\right)}$	(6)
4	Obtain optimal minimum variance estimate of the state vector and corresponding error covariance.	$\hat{x}_k \approx \sum_{i=1}^{N_s} w_{k|k}^{i} x_k^i$ $P_{\hat{x}_k} \approx \sum_{i=1}^{N_s} w_{k|k}^{i} (x_k^i - \hat{x}_k)(x_k^i - \hat{x}_k)^T$	(7)
5	Let k = k+1 & iterate to step 2.		
In the above equations it is required that the likelihood pdf $p(z_k|x_k^i)$ and the transitional probabilities $p(x_k^i|x_{k-1}^j)$ be known and specified.			

The q_c*HMM* algorithm implements a BRE smoother. BRE smoothing uses all measurements available to estimate the state of a system at a certain time or depth in the q_v estimation case (Arulampalam et al., 2002; Baziw and Verbeek, 2021, 2022A, and 2022B; Gelb, 1974). This requires both a forward and backward filter formulation. The forward HMM filter ($\hat{q}_k^F$) processes measurement data (q_m) above the cone tip ($j = 1\ to\ 30 \times \left(\frac{d_c}{\Delta}\right)$) in (1)). Next the backward HMM

filter ($\hat{q}_k^B$) is implemented, where the filter recurses through the data below the cone tip ($j = 30 \times \left(\frac{d_c}{\Delta}\right)$ *to* $60 \times \left(\frac{d_c}{\Delta}\right)$ in (1)) starting at the final q_m value. The optimal estimate for q_v is then defined as

$$\hat{q}_k^v = (\hat{q}_k^F + \hat{q}_k^B)/2 \tag{8}$$

where the index k represents each q_m measurement.

In both the forward and backward HMM filter formulation a bank of discrete $q_v$values (*i = 1 to N*) varying from low (q_{vL}) to high (q_{vH}) and a corresponding q_v resolution q_{vR} is specified. The required number of fixed grid HMM states is given as $N_S = (q_{vH} - q_{vL})/q_{vR}$. In Table 1, the notation of the states x^i is mapped to q^i to reflect the bank of $q_v$values.

In the q_m*HMM-IFM* HMM forward and backward filter formulation the transitional probabilities (i.e., $p\left(x_k^i | x_{k-1}^j\right)$ or $p\left(q_k^i | q_{k-1}^j\right)$) for each HMM state (i.e., discrete cone tip, $q^{,i}$) is set equal due to the fact that there is equal probability of moving from a current cone tip value to any other value between the range q_{vL} to q_{vH}. The likelihood PDF $p(z_k|q_k^i)$ in the HMM filter outlined in Table 1 is calculated based upon an assumed Gaussian measurement error as follows:

$$p(z_k|q_k^i) = \frac{1}{\sqrt{2\pi\sigma}} e^{\left[-\frac{\left(q_m(d) - z_k^i\right)}{2\sigma^2}\right]} \tag{10}$$

where σ^2 is the variance of the measurement noise. Baziw and Verbeek (2021) outline the details of the q_c*HMM* algorithm HMM forward and backward filter formulation. The current q_c*HMM* filter formulation no longer requires the setting of minimum and maximum limits of the q_v values (Baziw and Verbeek, 2022A).

q_c*HMM* VARYING CONE DIAMETER TEST BED SIMULATIONS

The performance of the q_c*HMM* algorithm was evaluated by carrying out a challenging test bed simulations. The simulated cone bearing profiles are generated for a true cone bearing profile q_v where acquired measured values q_c are obtained by implementing eq. (1) for cone tip areas of 5cm^2, 10cm^2, and 15cm^2.

Figure 2 illustrates a true cone bearing profile q_v (black trace) of a challenging soil profile containing variable thin layers. The measured values obtained by implementing eq. (1) for cone tip areas of 5cm^2 (red trace), 10cm^2 (green trace) and 15cm^2 (blue trace) are also illustrated in Fig. 2. As expected, a larger cone tip area/diameter will result in greater q_c blurring. Alternatively, relatively smaller area cone tips have cone bearing measurements which are more susceptible to anomalous peaks and troughs due to the relatively small diameter cone tip penetrating sandy, silty and gravelly soils (Baziw and Verbeek, 2022b). Figure 3 illustrates the output of the q_c*HMM* algorithm when processing the 5cm^2 q_c data. In Fig. 3, the black trace is the 5cm^2 q_c values, the red trace is the true cone bearing values q_v and the blue trace is the q_c*HMM* estimated cone bearing values $q_v^{,}$ (blue trace). As is shown in Fig. 3, the estimated $q_v^{,}$ values are nearly identical to the true values q_v for the 5cm^2 q_c data set.

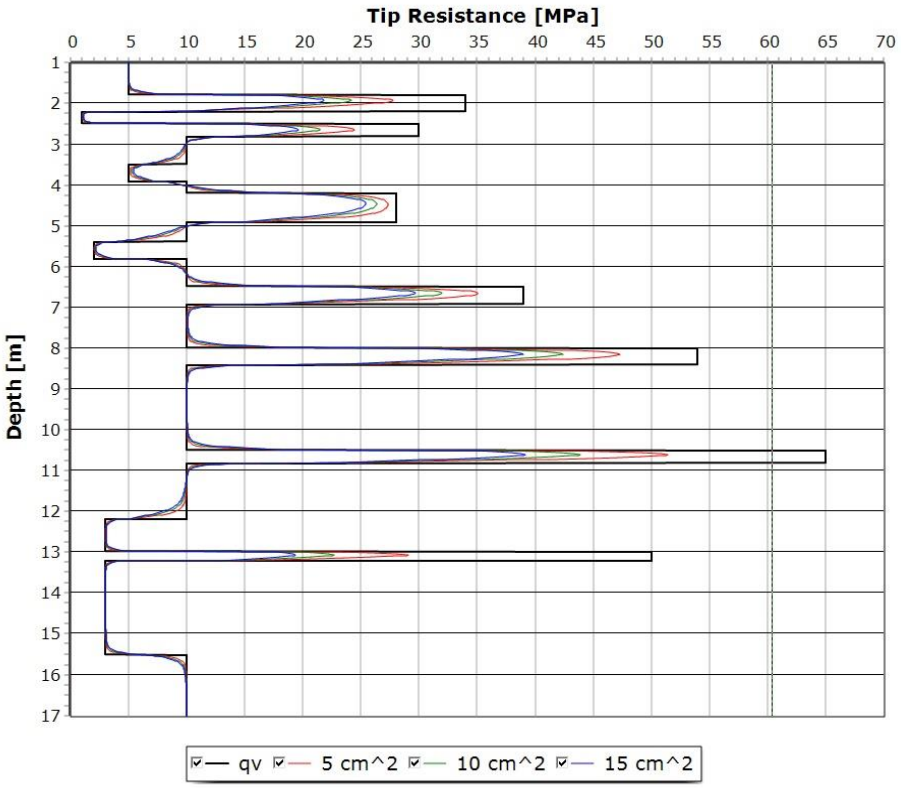

Figure 2. Specified q_v values (black trace) and derived q_c values for cone tip diameters of 5cm^2 (red trace), 10cm^2 (green trace) and 15cm^2 (blue trace).

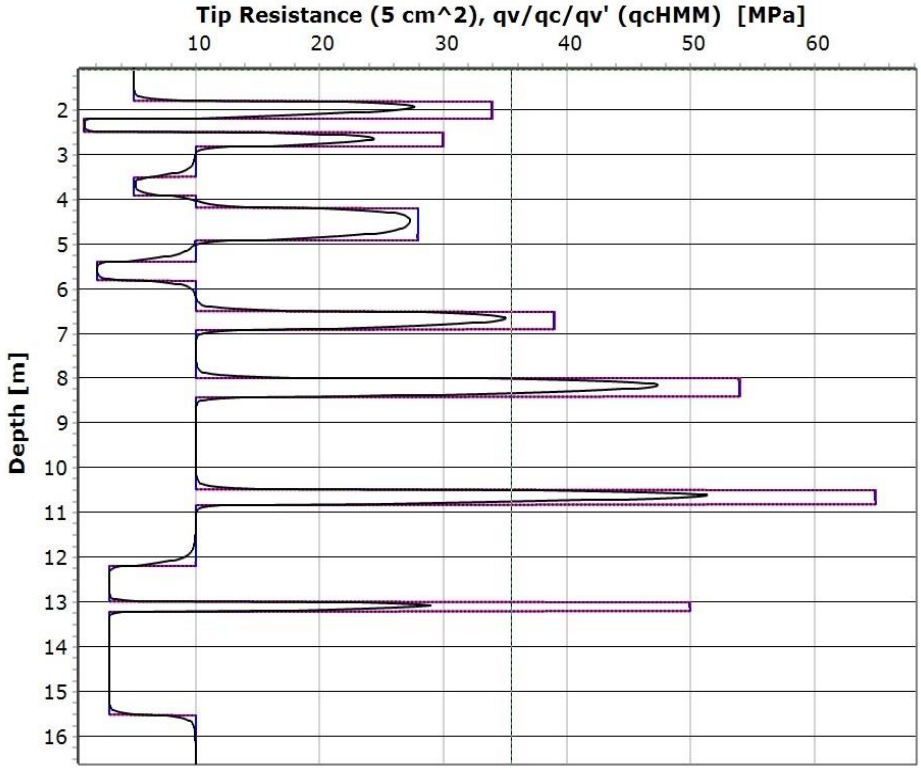

Figure 3. Specified q_c values (black trace), true cone bearing values q_v (red trace) and q_c*HMM* estimated cone bearing q_v' (blue trace) for the 5cm^2 cone tip.

Figure 4 illustrates the output of the q_c*HMM* algorithm when processing the 10cm^2 q_c data. In Fig. 4, the black trace is the 10cm^2 q_c values, the red trace is the true cone bearing values q_v and the blue trace is the q_c*HMM* estimated cone bearing values $q_v^{/}$ (blue trace). As is shown in Fig. 4, the estimated $q_v^{/}$ values are nearly identical to the true values q_v for the 10cm^2 q_c data set.

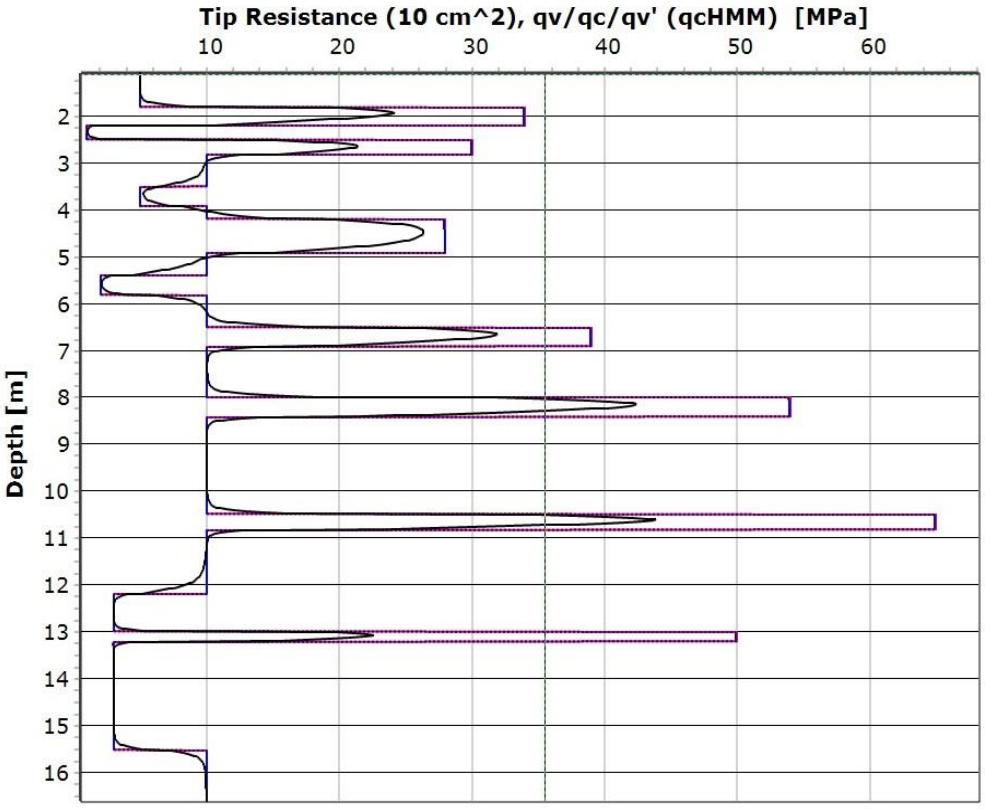

Figure 4. Specified q_c values (black trace), true cone bearing values q_v (red trace) and q_c*HMM* estimated cone bearing $q_v^{/}$ (blue trace) for the 10cm^2 cone tip.

Figure 5 illustrates the output of the q_c*HMM* algorithm when processing the 15cm^2 q_c data. In Fig. 5, the black trace is the 15cm^2 q_c values, the red trace is the true cone bearing values q_v and the blue trace is the q_c*HMM* estimated cone bearing values $q_v^{/}$ (blue trace). As is shown in Fig. 5, the estimated $q_v^{/}$ values are nearly identical to the true values q_v for the 15cm^2 q_c data set. Figure 6 illustrates the superposition of the true q_v values (black trace) and the q_c*HMM* estimated $q_v^{/}$ values for the 5cm^2 cone tip (red trace), 10cm^2 cone tip (green trace), and 15cm^2 cone tip (blue trace). As is evident in Fig. 6, the q_c*HMM* estimated $q_v^{/}$ values for the variable cone tip areas are nearly identical to the true values. This test bed simulation clearly demonstrates that the q_c*HMM* algorithm can be implemented so that q_c profiles obtained from cones with varying cone tip diameters can be corrected to give consistent\identical results.

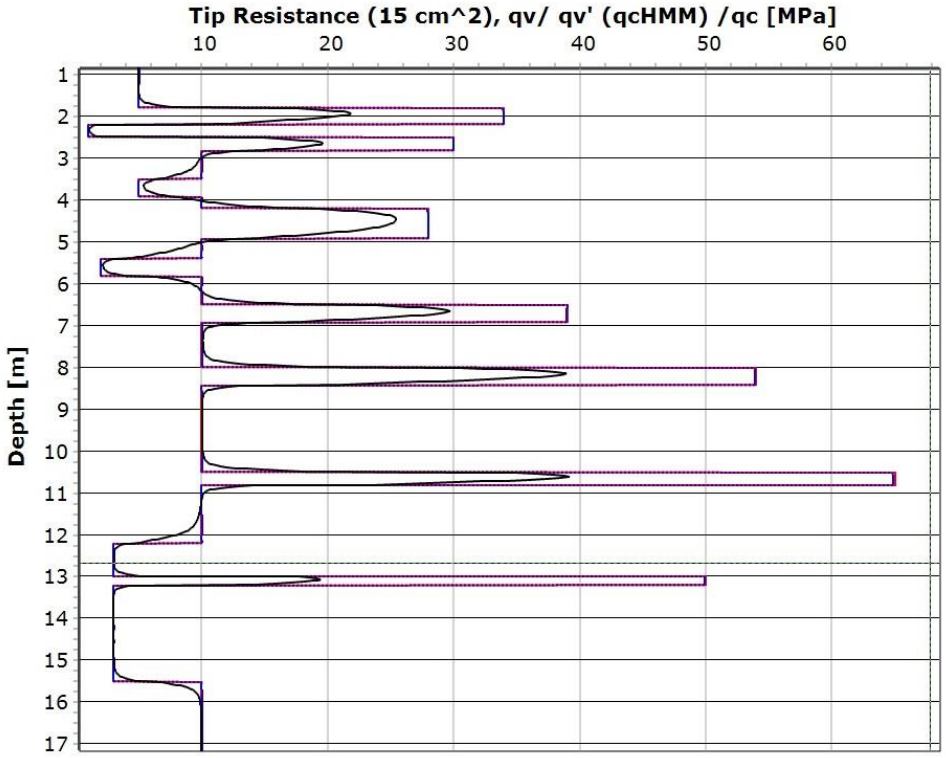

Figure 5. Specified q_c values (black trace), true cone bearing values q_v (red trace) and q_cHMM estimated cone bearing $q_v^{/}$ (blue trace) for the 15cm^2 cone tip.

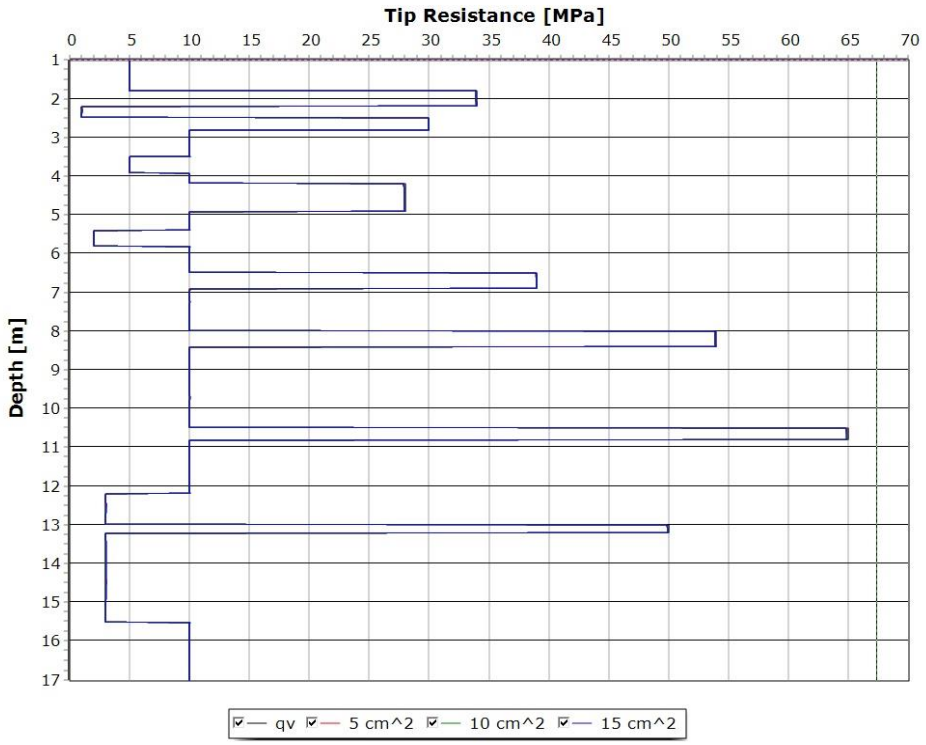

Figure 6. Specified true q_v values (black trace) and the q_cHMM estimated $q_v^{/}$ values for the 5cm^2 cone tip (red trace), 10cm^2 cone tip (green trace), and 15cm^2 cone tip (blue trace).

CONCLUSION

This paper outlines the current q_c*HMM* algorithm formulation. The q_c*HMM* algorithm was developed to address the cone bearing q_c blurring\averaging limitation where the resolution of a cone bearing profile can be significantly reduced. The q_c*HMM* algorithm implements a hidden Markov model smoother so that true cone bearing are obtained from the averaged/blurred q_c values. The cone tip diameter is directly related to the extent of blurring of the q_c values. A larger cone tip diameter will resulted in greater q_c blurring. The most common cone tips have associate areas of 5 cm^2, 10 cm^2 and 15 cm^2. A challenging test bed simulation outlined in this paper has clearly shown that the q_c*HMM* algorithm can be implemented so that q_c profiles obtained from cones with varying cone tip diameters can be corrected to give consistent\identical results.

REFERENCES

Arulampalam, M.S., Maskell, S., and Clapp, T. (2002). "A tutorial on particle filters for online nonlinear/non-Gaussian Bayesian tracking", IEEE Transactions on Signal Processing, vol. 50, no. 2, pp. 174-188, Feb. 2002.

ASTM D6067 / D6067M – 17 (2017). "Standard Practice for Using the Electronic Piezocone Penetrometer Tests for Environmental Site Characterization and Estimation of Hydraulic Conductivity", ASTM Vol. 4.09 Soil and Rock (II): D5877-latest.

Baziw, E. (2007), Application of Bayesian Recursive Estimation for Seismic Signal Processing, Ph.D. Thesis, Dept. of Earth and Ocean Sciences, University of British Columbia.

Baziw, E. and Verbeek, G. (2021). "Cone Bearing Estimation Utilizing a Hybrid HMM and IFM Smoother Filter Formulation", International Journal of Geosciences (IJG) Special Issue on Geoscientific Instrumentation, Methods and Data Systems, 10.4236/ijg.2021.1211055, Vol 12 (11), 1040-1054.

Baziw, E. and Verbeek, G. (2022a). " Identification of Thin Soil Layers Utilizing the qmHMM-IFM Algorithm on Cone Bearing Measurements", Geo-Congress 2022 (1st Edition), ASCE Press, https://doi.org/10.1061/9780784484036, 505 - 514.

Baziw, E. and Verbeek, G. (2022b). "Methodology for obtaining true cone bearing estimates from blurred and noisy measurements", Cone Penetration Testing 2022 (1st Edition), CRC Press, eBook ISBN9781003308829, 115-120.

Boulanger, R.W. and DeJong, T.J. (2018). "Inverse filtering procedure to correct cone penetration data for thin-layer and transition effects" Proc., Cone Penetration Testing 2018, Hicks, Pisano, and Peuchen, eds., Delft University of Technology, The Netherlands, 25-44.

Eslami, A., and Fellenius, B.H. (1995). "Toe bearing capacity of piles from cone penetration test (CPT) data", In Proceedings of the International Symposium on Cone Penetrometer Testing, CPT '95, Linkoping, Sweden, 4–5 October 1995. Swedish Geotechnical Society, Gothenburg, Sweden.

Eslami, A. and Fellenius, B.H. (1997). ''Pile capacity by direct CPT and CPTu methods applied to 102 case histories'', Canadian Geotechnical Journal(CGJ),6, 886–904.

Gelb, A. (1074), Applied Optimal Estimation (4th Edition), Cambridge, Mass: MIT Press.
Robertson, P.K. (1990), "Soil classification using the cone penetration test", Canadian Geotechnical Journal 27 (1), 151-158.